

Effects of Current Distribution on Mass Transport in the Positive Electrode of a Liquid Metal Battery

P. Personnettaz, S. Landgraf, M. Nimtz, N. Weber, T. Weier*

Helmholtz-Zentrum Dresden – Rossendorf, Bautzner Landstr. 400, Dresden, Germany

*Corresponding author: p.personnettaz@hzdr.de

Liquid metal electrodes are one of the key components of different electrical energy storage technologies. The understanding of transport phenomena in liquid electrodes is mandatory in order to ensure efficient operation. In the present study we focus our attention on the positive electrode of a Li||Bi liquid metal battery. Starting from a real experimental setup, we numerically investigate charge transfer in the molten salt electrolyte and mass transport in the positive electrode. The two phenomena are tightly coupled, because the current distribution influences the concentration field in the positive electrode. The cell is studied during charge, when compositional convection becomes apparent. First results of compositional convection from an inhomogeneous current distribution are presented, highlighting its capability to affect the flow in the positive electrode and the cell performance.

Introduction. Electrical energy storage (EES) is recognized as to be essential for a broader deployment of intermittent renewable sources in the electricity production. Liquid metal batteries (LMBs) [1, 2], sodium-sulfur [3] and liquid metal displacement batteries (LDBs) [4] are promising EES candidates. They all have in common a key component, the liquid metal electrode (LME). The fully fluid nature of LMEs guarantees simple construction (scale up) of the cell and extended lifetime [5]. Simultaneous charge, heat, mass and momentum transfer takes place in these electrodes and affects their electrochemical behavior. The actual knowledge of these phenomena is far from being comprehensive, despite the relatively simple geometry and chemistry. The high operating temperatures and the chemical aggressive environment limit the experimental study to few measurable quantities. Numerical studies based on continuum mechanics allow to infer the physics and to understand the relevant transport mechanisms.

The presence of high current density across conducting fluids (liquid metals) has promoted the investigation of multiple magnetohydrodynamic (MHD) phenomena [2]: liquid metal columns crossed by electrical current may be subject to the Taylor instability [6, 7]; interface instabilities can be excited by Lorentz forces [8]; diverging current distributions may lead to electrovortex flows [7, 9, 10, 11, 12]. Looking at non-uniform current distributions from a different perspective, motivated by an ongoing experiment and a previous work [13], in this study we want to investigate the effect on mass transport of an inhomogeneous current profile on the charging phase of a Li||Bi liquid metal battery.

In the experiments published so far the negative electrode has different shapes (spherical droplet [14], cylindrical porous matrix [15] or spiral [13]). In all of these setups the negative active surface is smaller with respect to the positive electrode-electrolyte interface. This affects the primary current distribution in the electrolyte and the mass flux at the top interface of the positive electrode. During charge, Li is removed (negative mass flux) from the top interface of the positive electrode (electrorefining) through a process of Li reduction and migration in the electrolyte

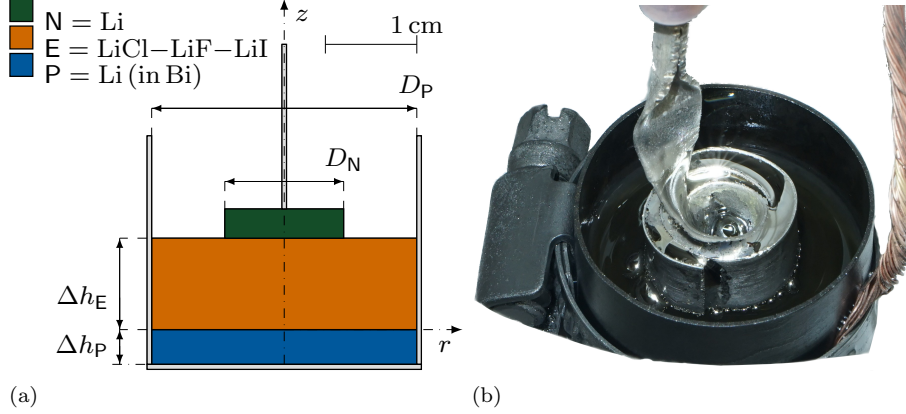


Figure 1: (a) Geometry of the experimental Li||Bi cell. (b) Experimental Li||Bi cell.

layer. This phenomenon generates denser fluid at the top part of the positive electrode. The density stratification is unstable and the fluid parcels sink down, thereby producing a compositional convective flow [2]. In the previous work we have assumed a uniform mass flux [13], here we study if this approximation is justified, and what effect it has on the estimation of the cell performance.

1. Experimental setup. The Li||Bi cell is composed of three liquid layers stratified by density, as shown in Fig. 1a. The positive electrode consists of a liquid alloy (Li(in Bi)) and it constitutes the lower layer. On top of that an eutectic LiCl–LiF–LiI molten salt electrolyte floats. Both layers are contained in a tantalum vessel, in order to minimize side reactions. The top lithium (Li) negative electrode is laterally confined in a nickel spiral, as shown in Fig. 1b. The concentration cell is open and immersed in a controlled Ar atmosphere, in order to ensure safety and optical access [14]. A heating plate placed on the bottom of the vessel keeps the cell core temperature of about 460 °C. The geometrical parameters and the relevant material properties are compiled in Tab 1.

Table 1: Relevant geometrical parameters of the Li||Bi LMB; thermodynamic and transport properties of the Li(in Bi) alloy and LiCl–LiF–LiI molten salt electrolyte at $T = 460\text{ °C}$ [16, 17, 18, 19, 20].

diameter of the inner vessel	D_P	29 mm
diameter of the negative electrode	D_N	13 mm
thickness of the molten salt layer	Δh_E	10 mm
thickness of the positive electrode	Δh_P	3.8 mm
mixture density	$\rho_{\text{tot,ref}}$	$8.2 \times 10^3 \text{ kg m}^{-3}$
compositional expansion coefficient	β_ρ	$1.88 \times 10^{-3} \text{ m}^3 \text{ kg}^{-1}$
reference mass concentration of Li	$\rho_{A,\text{ref}}$	$9.045 \times 10^1 \text{ kg m}^{-3}$
kinematic viscosity	ν	$1.31 \times 10^{-7} \text{ m}^2 \text{ s}^{-1}$
diffusion coefficient of Li in Bi	\mathcal{D}_{AB}	$5 \times 10^{-9} \text{ m}^2 \text{ s}^{-1}$
molar mass of Lithium	\mathcal{M}_A	$6.941 \times 10^{-3} \text{ kg mol}^{-1}$
ionic conductivity of the electrolyte	$\sigma_{\text{el, E}}$	$2.71 \times 10^2 \text{ S m}^{-1}$

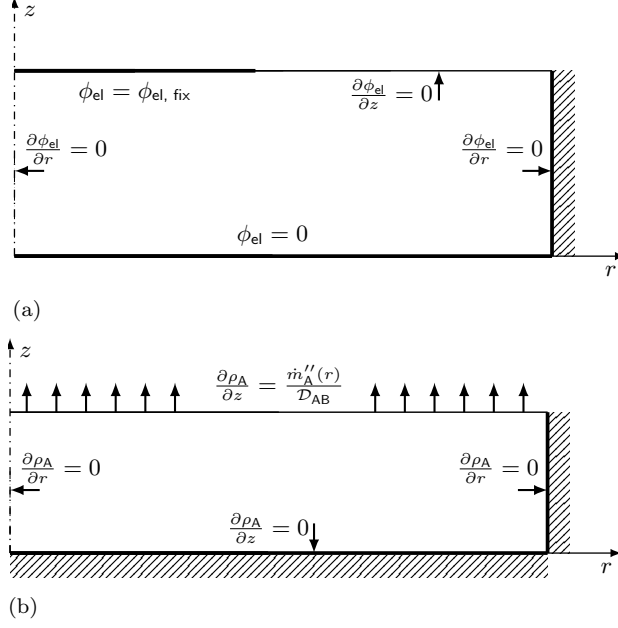


Figure 2: (a) Electrolyte (axial symmetry), boundary conditions for the primary current distribution. (b) Positive electrode (axial symmetry), boundary conditions for the mass transport equation.

2. Numerical model In order to study the effect of an inhomogeneous current density on the Li-concentration distribution we first solve the electro-dynamics problem and then we apply the derived current profile as boundary condition for mass transport in the positive electrode. In order to simplify the model and to reduce the numerical effort we use the axisymmetric approximation.

2.1. Electrostatics The primary current distribution at the interface between the electrolyte and the positive electrode $j(r, z = 0) = j(r)$ can be numerically computed from the solution of the Laplace equation for the electric potential ϕ_{el} in the electrolyte:

$$\nabla \cdot \sigma_{\text{el, E}} \nabla \phi_{\text{el}} = 0, \quad (1)$$

in which $\sigma_{\text{el, E}}$ is the ionic conductivity of the molten salt. We assume a Dirichlet boundary condition for the interfaces between electrolyte and liquid metals and a homogeneous Neumann boundary condition elsewhere, as shown in Fig. 2a. The current density \mathbf{j} is derived from the Ohm law, $\mathbf{j} = -\sigma_{\text{el, E}} \nabla \phi_{\text{el}}$. The solution was computed with the Laplace solver of the free and open source CFD library **OpenFOAM** and is presented in Fig. 3. These results were compared with the primary current distribution in the full cell and an excellent agreement was confirmed for the current density at the electrolyte-positive electrode interface. Eq. 1 can be solved analytically as well in the form of an infinite sum of Bessel functions. We use a polynomial fit of the fifth order to interpolate the radial dependence of the current profile $j(r) = \langle j \rangle \cdot \sum_{i=0}^5 a_i \cdot r^i$.

2.2. Mass transport We study concentration and flow fields in the positive electrode with a single phase-single region model. The following assumptions are

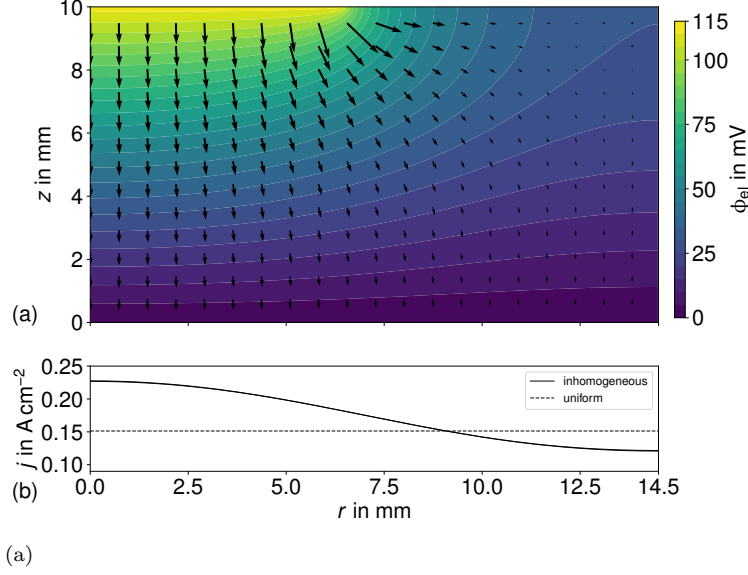


Figure 3: (a) Electric potential $\phi_{\text{el}}(r, z)$ and current density $\mathbf{j}(r, z)$ distribution in the electrolyte. (b) Current density profile $j(r, z = 0)$ at the interface between electrolyte and positive electrode for $I = 1 \text{ A}$.

used: isothermal conditions; rigid and flat interface with the molten salt electrolyte. The concentration distribution is modeled with the advection-diffusion equation:

$$\frac{\partial \rho_A}{\partial t} + \mathbf{u} \cdot \nabla \rho_A = \nabla \cdot \mathcal{D}_{AB} \nabla \rho_A \quad (2)$$

in which ρ_A is the mass concentration of the component A (Li), \mathbf{u} is the velocity field and \mathcal{D}_{AB} is the diffusion coefficient [21]. The boundary conditions (BCs) for mass transport are shown in Fig. 2b. We consider two configurations: a uniform (a) and an inhomogeneous (b) mass flux at the top interface \dot{m}''_A :

$$(a) \quad \dot{m}''_A = \frac{\langle j \rangle \mathcal{M}_A}{n_{\text{el}} F \mathcal{D}_{AB}} \quad (b) \quad \dot{m}''_A(r) = \frac{j(r) \mathcal{M}_A}{n_{\text{el}} F \mathcal{D}_{AB}} = \frac{\langle j \rangle \mathcal{M}_A}{n_{\text{el}} F \mathcal{D}_{AB}} \sum_{i=0}^5 a_i \cdot r^i \quad (3)$$

in which $\langle j \rangle$, F , \mathcal{M}_A , n_{el} , are mean current density, Faraday constant, molar mass of Li and the number of electrons transferred per ion ($n_{\text{el}} = 1$) respectively. The mean current density is calculated with the positive electrode area ($\langle j \rangle = \frac{4 \cdot I}{\pi D_p^2}$). The velocity field \mathbf{u} is computed by solving the incompressible Navier-Stokes equations in the Boussinesq approximation: the continuity equation,

$$\nabla \cdot \mathbf{u} = 0, \quad (4)$$

and the momentum equation,

$$\frac{\partial \mathbf{u}}{\partial t} + (\mathbf{u} \cdot \nabla) \mathbf{u} = -\frac{1}{\rho_{\text{tot, ref}}} \nabla p + \nu \nabla^2 \mathbf{u} + \mathbf{g}(1 - \beta_\rho (\rho_A - \rho_{A, \text{ref}})), \quad (5)$$

in which p , $\rho_{\text{tot, ref}}$, ν , \mathbf{g} , β_ρ are pressure, total mixture density, kinematic viscosity, gravitational acceleration and composition coefficient of volume expansion [22]. The density of the alloy is calculated with Vegard's law [23]. We apply a no-slip

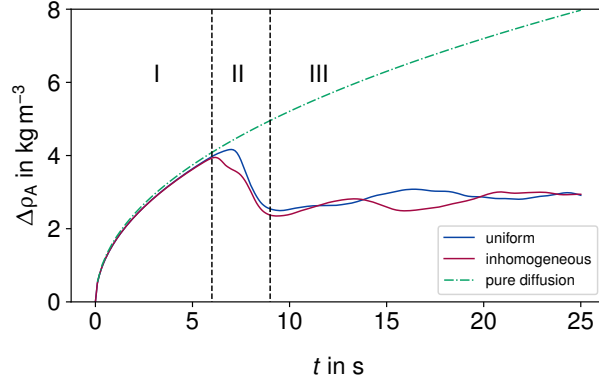


Figure 4: Evolution of the concentration difference between the bulk fluid and the interface for $I = 1$ A ($\Delta\rho_A(t) = \langle\rho_A\rangle_V(t) - \langle\rho_A\rangle_S(t)$).

condition at the solid boundaries and at the interface with the electrolyte layer. We ensure the symmetry condition on the z -axis. The numerical model is implemented in `OpenFOAM`, by extending the `buoyantBoussinesqPimpleFoam` solver. The inhomogeneous current boundary condition generates an uneven current distribution in the liquid metal layer. The interaction of the current with its own induced magnetic field leads to a Lorentz force distribution with a non-vanishing rotational part. Such a force field can drive a fluid flow, known as electrovortex flow (EVF). In the work of Herreman et al. [24] it is shown that compositional convection exceeds EVF in a parameter range similar to the one studied. Furthermore, in our experiment the current profile at the interface is smoother with respect to the ones studied by Herreman et al. [12, 24]. Therefore, we expect an even weaker EVF. Due to these considerations, we neglect its contribution, and we assume that magnetohydrodynamic effects are negligible. In the case of an externally applied magnetic field, the validity of this assumption should be carefully verified [11].

3. Results and discussion In this section we present first results on compositional convection in the positive electrode under the effect of a uniform and an inhomogeneous mass flux. During charge the liquid alloy behaves like a viscous fluid cooled from the top surface (e.g. evaporative cooling [25]). The mass flux removes Li from the Li (in Bi) alloy, which generates continuously a locally denser fluid. The phenomenon studied is intrinsically unsteady due to the flux boundary condition.

The flow shows a topology that is totally different from the organized motion typical for EVFs [12]. This is due to the absence of a “basically stationary” body force field ($\mathbf{j} \times \mathbf{B}$). The buoyancy term affecting the flow field shows an uneven and transient behavior due to the strong coupling with the mass transport equation and its BCs.

We can qualitatively distinguish three different behaviors during compositional convection. Initially the concentration boundary layer starts to form but the fluid remains at rest in a quasi stable regime [26], it is diffusion dominated (Fig. 4, $\rho_A(t) \propto \sqrt{t}$). Then, in the second regime, the denser layer becomes unstable and plumes begin to detach from the top interface; the penetration decelerates the heavy fluid, generating the classical mushroom shape, with vortex rings and more complex structures, as shown in Fig. 5.

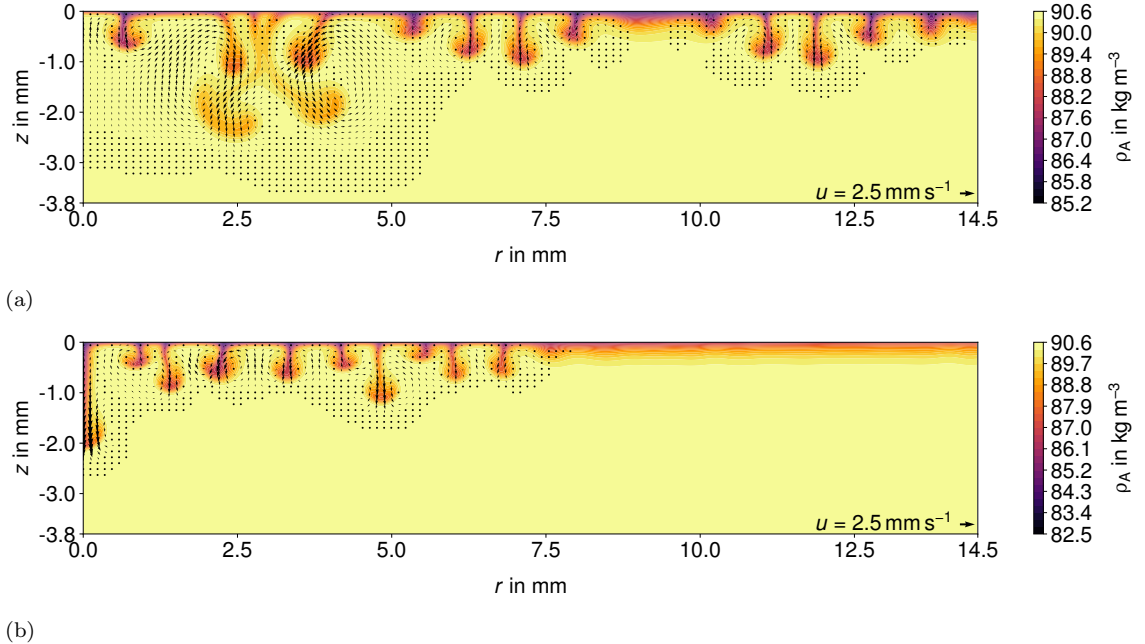


Figure 5: Instantaneous concentration and velocity fields in the positive electrode of a Li||Bi LMB for $I = 1 \text{ A}$. (a) Uniform current distribution at $t = 7.5 \text{ s}$, (b) inhomogeneous current distribution at $t = 6.5 \text{ s}$.

The presence of an inhomogeneous current distribution affects time and location of the onset of the compositional convection. In this condition instability starts in the center of the cell, as shown in Fig. 5b; the threshold limit for convection is reached earlier (e.g. $\sim 2 \text{ s}$ for $I = 1 \text{ A}$) and the peripheral region remains fluid-dynamically stable and purely diffusive in the first seconds. In the uniform case compositionally driven motion begins everywhere affecting rapidly the top region of the layer, see Fig. 5a. When the concentration perturbation has reached the bottom of the electrode, large scale structures appear, as shown in Fig. 6; the presence of walls becomes relevant and the acceleration of the flow decreases. In this third regime the effect of the inhomogeneous current distribution is less evident due to the presence of large scale unsteady and chaotic structures that affect the full layer. If we analyse the evolution of the difference between the average mass concentration at the interface and in the volume $\Delta\rho_A$ we cannot observe relevant differences between the uniform and inhomogeneous current distribution, especially in the last region when it becomes stable (Fig. 4). This concentration difference is directly connected with the mass transport overpotential, as described in [13], we can therefore conclude that the inhomogeneous current distribution that we studied has no relevant impact on the performance of the cell.

4. Conclusions We have developed a numerical model able to describe mass transport in the positive electrode of liquid metal batteries, under different current distributions. In the range of parameters studied we could numerically confirm that the different electrodes areas, typical for experimental cells, have a negligible impact on the cell performance during charge. They only affect fluid flow and the concentration distribution in the first seconds when compositional convection sets in. A detailed investigation on a large range of operating param-

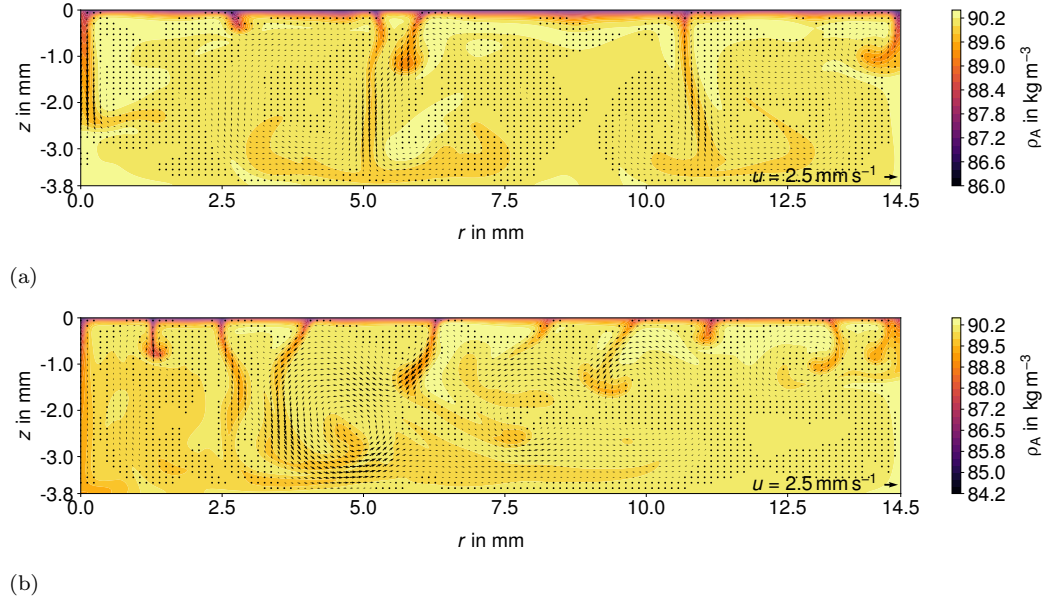


Figure 6: Instantaneous concentration and velocity fields in the positive electrode of a Li||Bi LMB for $I = 1$ A. (a) Uniform and (b) inhomogeneous current distribution at $t = 15$ s.

ters is currently ongoing. Further studies will be oriented to study the validity of the 2D approximation with fully three-dimensional simulations and to investigate the effect of the mechanical interaction with the electrolyte layer. Furthermore, the presence of a non-uniform current distribution has magneto-hydrodynamic implications that will be included in the future studies.

Acknowledgements. This work was supported by the Deutsche Forschungsgemeinschaft (DFG, German Research Foundation) by award number 338560565 and in frame of of the Helmholtz - RSF Joint Research Group “Magneto-hydrodynamic instabilities: Crucial relevance for large scale liquid metal batteries and the sun-climate connection”, contract No HRSF-0044 and RSF-18-41-06201. The computations were performed on the HPC-Cluster at the Center for Information Services and High Performance Computing (ZIH) at TU Dresden and on the HPC-Cluster “Hemera” at Helmholtz-Zentrum Dresden – Rossendorf.

REFERENCES

1. H. KIM, ET AL. Liquid metal batteries: Past, present, and future. *Chemical Reviews*, vol. 113 (2013), no. 3, pp. 2075–2099.
2. D. H. KELLEY AND T. WEIER. Fluid mechanics of liquid metal batteries. *Applied Mechanics Reviews*, vol. 70 (2018), no. 2, 020801.
3. K. B. HUESO, M. ARMAND, AND T. ROJO. High temperature sodium batteries: Status, challenges and future trends. *Energy & Environmental Science*, vol. 6, no. 3, p. 734.
4. H. YIN, ET AL. Faradaically selective membrane for liquid metal displacement batteries. *Nature Energy*, vol. 3 (2018), no. 2, pp. 127–131.
5. H. LI, ET AL. Liquid metal electrodes for energy storage batteries. *Advanced Energy Materials*, vol. 6 (2016), no. 14, 1600483.

6. N. WEBER, V. GALINDO, F. STEFANI, AND T. WEIER. Current-driven flow instabilities in large-scale liquid metal batteries, and how to tame them. *Journal of Power Sources*, vol. 265 (2014), pp. 166–173.
7. N. WEBER, ET AL. The Influence of Current Collectors on Tayler Instability and Electro-Vortex Flows in Liquid Metal Batteries. *Physics of Fluids*, vol. 27 (2015), no. 1, 014103.
8. N. WEBER, ET AL. Sloshing Instability and Electrolyte Layer Rupture in Liquid Metal Batteries. *Physics of Fluids*, vol. 29 (2017), no. 5, 054101.
9. R. F. ASHOUR, ET AL. Competing forces in liquid metal electrodes and batteries. *Journal of Power Sources*, vol. 378 (2018), pp. 301–310.
10. N. WEBER, ET AL. Electromagnetically driven convection suitable for mass transfer enhancement in liquid metal batteries. *Applied Thermal Engineering*, vol. 143 (2018), pp. 293–301.
11. N. WEBER, ET AL. Numerical simulation of mass transfer enhancement in liquid metal batteries by means of electro-vortex flow. *Journal of Power Sources Advances*, vol. 1 (2020), 100004.
12. W. HERREMAN, ET AL. Numerical simulation of electrovortex flows in cylindrical fluid layers and liquid metal batteries. *Physical Review Fluids*, vol. 4 (2019), no. 11, 113702.
13. P. PERSONNETTAZ, ET AL. Mass transport induced asymmetry in charge/discharge behavior of liquid metal batteries. *Electrochemistry Communications*, vol. 105 (2019), 106496.
14. T. WEIER, ET AL. Liquid metal batteries - materials selection and fluid dynamics. *IOP Conference Series: Materials Science and Engineering*, vol. 228 (2017), 012013.
15. K. WANG, ET AL. Lithium-antimony-lead liquid metal battery for grid-level energy storage. *Nature*, vol. 514 (2014), pp. 348–350.
16. C. FAZIO, ET AL. Handbook on lead-bismuth eutectic alloy and lead properties, materials compatibility, thermal-hydraulics and technologies, 2015.
17. R. W. OHSE ET AL. *Handbook of thermodynamic and transport properties of alkali metals* (Blackwell Oxford, 1985).
18. N. TEMNOGOROVA, I. VOLFSO, A. DEMIDOV, AND A. MORCHEVSKII. Determination of diffusion coefficients of lithium in molten alloys by anode chronopotentiometry. *Elektrokhimiya*, vol. 16 (1980), no. 3, pp. 419–421.
19. J. M. NEWHOUSE. Modeling the operating voltage of liquid metal battery cells. Ph.D. thesis, Massachusetts Institute of Technology, 2014.
20. P. MASSET AND R. A. GUIDOTTI. Thermal activated (thermal) battery technology. *Journal of Power Sources*, vol. 164 (2007), no. 1, pp. 397–414.
21. R. B. BIRD, W. E. STEWART, AND E. N. LIGHTFOOT. *Transport Phenomena* (2002).
22. L. G. LEAL. *Advanced Transport Phenomena: Fluid Mechanics and Convective Transport Processes*. Cambridge Series in Chemical Engineering (Cambridge University Press, 2007).
23. L. VEGARD. Die Konstitution der Mischkristalle und die Raumfüllung der Atome. *Zeitschrift für Physik*, vol. 5 (1921), no. 1, pp. 17–26.
24. W. HERREMAN, ET AL. Solutal buoyancy and electrovortex flow in liquid metal batteries. *submitted to Physical Review Fluids*, (2020).
25. T. D. FOSTER. Onset of convection in a layer of fluid cooled from above. *Physics of Fluids*, vol. 8, no. 10, p. 1770.
26. T. D. FOSTER. Onset of manifest convection in a layer of fluid with a time-dependent surface temperature. *Physics of Fluids*, vol. 12, no. 12, p. 2482.